Wave-Vector-Dependent Exciton Exchange Interaction

G. Dasbach,[1] D. Fröhlich,[1] H. Stolz,[2] R. Klieber,[1] D. Suter,[1] and M. Bayer[1]
[1]*Institut für Physik, Universität Dortmund, D-44221 Dortmund, Germany*
[2]*Fachbereich Physik, Universität Rostock, D-18051 Rostock, Germany*
(Received 8 April 2003; published 4 September 2003)

The exchange interaction for the yellow $1S$ orthoexciton in Cu_2O is derived up to the order K^2. The resulting exchange splittings are verified experimentally using high resolution spectroscopy. In agreement with theory the fine structure shows a characteristic dependence on the direction of the wave vector.

DOI: 10.1103/PhysRevLett.91.107401 PACS numbers: 78.20.–e, 71.35.Cc, 78.40.Fy

Exchange interaction couples the spins of electron and hole, which gives rise to an exciton fine structure. This fine structure has been studied intensely. Investigations beginning with bulk semiconductors [1,2] have been extended to quantum wells [3] and recently further to quantum dots [4]. Exchange interaction splits excitonic levels of different total angular momenta. Because of the complexity of the semiconductor band structure difficulties in calculating the electron-hole exchange microscopically arise. Attempts to describe it on a quantitative level can hardly be found [5]. In higher dimensional structures exchange interaction is normally treated as a wave vector independent spin-spin interaction, which is in agreement with the experiments reported so far. These studies, however, were performed with modest spectral resolution of typically $\gtrsim 20$ μeV. Spectroscopic studies of exchange are often difficult as the energy splittings involved are rather small. In addition, difficulties arise from a limited crystal quality. Cu_2O is the prototype material for exciton physics [6], due to its high crystal quality and large binding energy of 150 meV. Hence, it seems ideally suited for the study of electron-hole exchange and its wave vector ($\mathbf{K}$) dependence.

In this Letter, we present transmission studies of the $1S$ ground state of the yellow exciton series in Cu_2O. Using a single frequency dye laser we achieve a spectral resolution of ≈ 5 neV. At this extreme resolution the linewidth of the transition is found to be much smaller than measured previously (< 1 μeV FWHM at $T = 1.4$ K). More strikingly, the orthoexciton, so far treated as threefold degenerate in unstrained samples, shows a characteristic fine structure, where the splitting critically depends on the direction of the wave vector. We demonstrate that the fine structure arises from $\mathbf{K}$-dependent exchange interaction, to our knowledge never observed before in any excitonic system.

The yellow $1S$ excitons are formed by a hole in the valence band (Γ_7^+) and an electron in the conduction band (Γ_6^+). Consequently, the exciton is decomposed into a Γ_2^+ and a Γ_5^+ representation [7]. The so-called paraexciton (Γ_2^+) is optically forbidden. The threefold orthoexciton (Γ_5^+) is quadrupole allowed [8], leading to a small oscillator strength and little radiative broadening as compared to dipole-allowed transitions [9].

Despite the quadrupole character, the exciton-photon interaction leads to coupled modes, the polaritons. Their dispersion depends on the exciton oscillator strength and $\mathbf{K}$. The amplitudes (QA_1 to QA_3) of the orthoexciton quadrupole transitions are given by the symmetric vector product of $\mathbf{K}$ and the polarization vector $\mathbf{e}$ [8]:

$$\begin{pmatrix} QA_1 \\ QA_2 \\ QA_3 \end{pmatrix} = \begin{pmatrix} e_y K_z + e_z K_y \\ e_z K_x + e_x K_z \\ e_x K_y + e_y K_x \end{pmatrix}. \tag{1}$$

We will now derive the electron-hole exchange up to the order K^2. It is given by the Coulomb interaction of the charge distributions ρ and ρ' [1],

$$J_{ex} = \delta_{\mathbf{K},\mathbf{K}'} \sum_{\mathbf{R}} e^{i\mathbf{K}\cdot\mathbf{R}} \iint \frac{\rho^*(\mathbf{r}_1)\rho'(\mathbf{r}_2) d\mathbf{r}_1 d\mathbf{r}_2}{|\mathbf{r}_1 + \mathbf{r}_2 - \mathbf{R}|}, \tag{2}$$

with the lattice vectors $\mathbf{R}$, where the orthoexciton exchange is determined by the interaction of the spin-singlet exciton charge distributions. Introducing the Fourier transform $M(\mathbf{K}) = \int d\mathbf{r}\rho(\mathbf{r}) \exp(-i\mathbf{K}\cdot\mathbf{r})$, the exchange integral is transformed into a sum over the reciprocal lattice vectors $\mathbf{K}_n$ [1],

$$J_{ex} = \delta_{\mathbf{K},\mathbf{K}'} \frac{4\pi}{\Omega} \sum_n \frac{M^*(\mathbf{K} + \mathbf{K}_n) M'(\mathbf{K} + \mathbf{K}_n)}{(\mathbf{K} + \mathbf{K}_n)^2}. \tag{3}$$

First, we concentrate on the long-range (LR) exchange ($\mathbf{K}_n = 0$). Expanding $\exp(-i\mathbf{K}\cdot\mathbf{r})$ into spherical harmonics $Y_{l,m}$ and decomposing ρ into multipoles [10], the LR quadrupole-quadrupole ($l = 2$) exchange energy is given by

$$J_{ex}^{Q} = \delta_{\mathbf{K},\mathbf{K}'} \frac{16\pi^2}{45\Omega} K^2 \sum_{m_{1,2}=-2}^{2} q_{m_1}^* q_{m_2} Y_{2,m_1}^*(\theta, \phi) Y_{2,m_2}(\theta, \phi), \tag{4}$$

where θ and ϕ are the spherical angles of $\mathbf{K}$ with respect to the cubic axes and $q_m = \sqrt{4\pi/5} \int d\mathbf{r} r^2 Y_{2,m}^* \rho(\mathbf{r})$ denote the quadrupole moments [10]. Then the matrix

representation of the exchange energy in the Cartesian orthoexciton basis $\Gamma_{5yz}^{+}, \Gamma_{5zx}^{+}, \Gamma_{5xy}^{+}$ is given by

$$J_{ex}^{Q} = \Delta_Q \cdot \frac{1}{K^2} \begin{pmatrix} K_z^2 K_y^2 & K_z^2 K_x K_y & K_z K_x K_y^2 \\ K_z^2 K_x K_y & K_z^2 K_x^2 & K_x^2 K_y K_z \\ K_z K_x K_y^2 & K_x^2 K_y K_z & K_x^2 K_y^2 \end{pmatrix}, \quad (5)$$

where Δ_Q is the LR quadrupole-quadrupole exchange parameter. In contrast to dipole-allowed excitons, the quadrupole LR exchange scales as K^2 and is therefore analytic at $\mathbf{K} = 0$. The paraexciton has zero spin-singlet charge density and hence is not affected by this interaction [11].

The $\mathbf{K}_n \neq 0$ terms of Eq. (3) give the short-range (SR) exchange, which we expand into orders of $\mathbf{K}$ and treat each order by the method of invariants [1,12]. The well known $\mathbf{K}$-independent SR contribution splits the paraexciton from the orthoexcitons by $\Delta_0 = 12$ meV [13]; however, it leaves the orthoexcitons degenerate. The next higher order term would scale linearly with $\mathbf{K}$, but vanishes due to the inversion symmetry of the lattice (point group O_h). The SR exchange of order K^2 gives nonvanishing contributions: The electron and hole spins transform as Γ_4^+, while $\mathbf{K}$ is a polar vector (Γ_4^-). Consequently, the SR exchange is given by representations of Γ_1^+, Γ_3^+, Γ_4^+, and Γ_5^+ [7]. The corresponding matrix representations J_1, J_3, J_4, and J_5 are given below.

$J_1 = \Delta_1 K^2 \cdot \mathbf{1}$ causes a rigid shift of all orthoexciton states by an energy Δ_1. It leads to an isotropic correction of the spatial dispersion and hence of the effective mass. J_3 is given by

$$J_3 = \Delta_3 \cdot \begin{pmatrix} 3K_x^2 - K^2 & 0 & 0 \\ 0 & 3K_y^2 - K^2 & 0 \\ 0 & 0 & 3K_z^2 - K^2 \end{pmatrix}. \quad (6)$$

It has diagonal form, where the states have a distinctive $\mathbf{K}$ dependence. Though J_3 gives rise to an orthoexciton fine structure, no mixing of the states occurs. J_4 vanishes as $\mathbf{K}$ transforms as Γ_4^-. Finally, J_5 is given by

$$J_5 = \Delta_5 \cdot \begin{pmatrix} 0 & K_x K_y & K_x K_z \\ K_x K_y & 0 & K_y K_z \\ K_x K_z & K_y K_z & 0 \end{pmatrix}. \quad (7)$$

J_5 has only off-diagonal terms and hence causes a $\mathbf{K}$-dependent mixing of the states. To summarize, we have derived three terms of order K^2 that can give rise to an orthoexciton fine structure: the LR quadrupole interaction J_Q^{ex}, and the SR contributions J_3, J_5, where the absolute splittings are determined by the exchange parameters Δ_Q, Δ_3, and Δ_5.

The $\mathbf{K}$ dependence of the exchange can be investigated experimentally by an absorption experiment, where the laser beam propagating along $\mathbf{K}$ directly probes the corresponding fine structure. The $\mathbf{K}$ dependence of the exchange has not been resolved in experiments with limited spectral resolution ($\gtrsim 20$ μeV). Thus the exchange splittings are expected not to be larger than a few μeV. To obtain such high resolution, we made use of a dye ring laser with a linewidth of ≈ 5 neV. The transmission was recorded while the laser energy was scanned across the orthoexciton resonances centered around 2.0327 eV. The absolute laser energy was adjusted within an accuracy of ≈ 10 μeV by means of a wave meter. The measurements were performed on high-quality natural Cu_2O crystals, which were oriented by x-ray diffraction. After cutting and polishing most crystals had a cubic shape with extensions of ≈ 4 mm. The samples were excited by linearly polarized light $\mathbf{e}(\psi)$, where the polarization angle ψ could be adjusted ($\psi = 0$ corresponds to horizontal $\mathbf{e}$). Polarizers placed in front of the sample and between sample and detector ensured precise control of the exciting as well as detected polarization components. Both polarizers were kept parallel. By adjusting $\mathbf{e}(\psi)$, the relative amplitudes of the orthoexciton states could be controlled [Eq. (1)]. Rotating the samples around the vertical axis by an angle φ' gave access to intermediate K directions. The dependence of the orthoexciton energies E_1, E_2, and E_3 on φ (angle of laser beam inside the sample) could thus be measured. Special care was taken to ensure a strain free mounting in the helium bath cryostat ($T = 1.4$ K).

For high symmetry $\mathbf{K}$'s the matrices (5)–(7) can be diagonalized analytically. For $\mathbf{K} = (\bar{1}10)$ exchange interaction should lift the degeneracy of the orthoexcitons and three separate lines are expected [Fig. 1(a)]. This is investigated by the experiments presented in Fig. 2. Calculating $|QA_2|^2$ shows that for $\psi = -36°$ [$\mathbf{e}(-36°) = (00\bar{1})$] the transition E_2 is maximally allowed [Fig. 2(a)]. One indeed finds a strong absorption [full line in Fig. 2(c)] [14]. For $\psi = +54°$ the E_2 transition is forbidden, as confirmed by the experiment [triangles in Fig. 2(c)]. The transitions E_1 and E_3 are forbidden for all ψ. For $\varphi \neq 0$ and $\psi = +54°$, however, E_1 and E_3 should become weakly allowed, while E_2 remains forbidden [Fig. 2(b)].

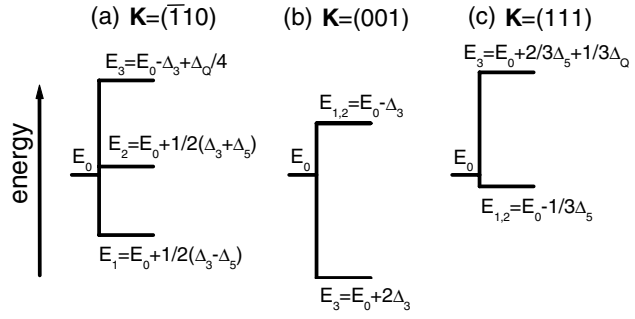

FIG. 1. Schematic energy level diagram of the exciton states. E_0 gives the orthoexciton energy including the exchange shifts Δ_0 and Δ_1. (a), (b), and (c) give the energy schemes for $\mathbf{K} = (\bar{1}10)$, (001), and (111), respectively, ($\Delta_Q = 5$ μeV, $\Delta_3 = -1.3$ μeV, $\Delta_5 = 2$ μeV).

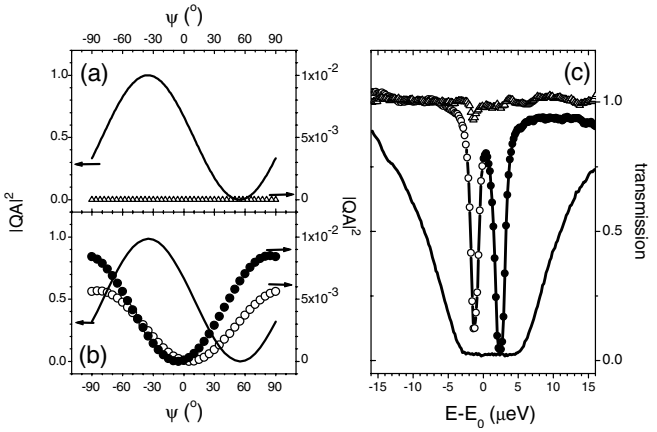

FIG. 2. (a) Calculated intensities $|QA_1|^2$, $|QA_3|^2$ (triangles), and $|QA_2|^2$ (full line) as a function of ψ for $\varphi = 0$. $\mathbf{K}(\varphi = 0)$ is along $(\bar{1}10)$ and for $\psi = 0$ the polarization vector $\mathbf{e}(\psi)$ points along $(11\bar{2})$. (b) Calculated intensities $|QA_2|^2$ (full line), $|QA_1|^2$ (open dots), and $|QA_3|^2$ (full dots) as a function of ψ for $\varphi = 4°$. Note the different scales for $|QA_1|^2$, $|QA_3|^2$ (right scale), and $|QA_2|^2$ (left scale). (c) Transmission spectra of a 4 mm thick crystal. The full line and the triangles show the transmission spectra for $\psi = -36°$ [$\mathbf{e} = (00\bar{1})$] and $\psi = 54°$ [$\mathbf{e} = (110)$], respectively, ($\varphi = 0$). The spectrum for $\psi = 54°$ and $\varphi = 4°$ [rotation around (111) axis] is shown by open dots [E_1 resonance in Fig. 1(a)] and full dots [E_3 resonance in Fig. 1(a)].

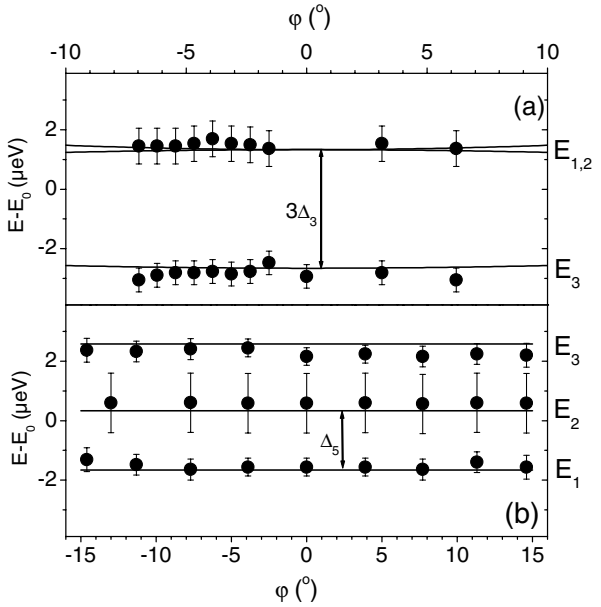

FIG. 3. E_1, E_2, E_3 as a function of φ for 4 mm thick samples. Dots mark the experimental data. Full lines give the calculated values. (a) For $\varphi = 0$, $\mathbf{K}$ is along (001). φ describes a rotation around the $(1\bar{1}0)$ axis. (b) For $\varphi = 0$, $\mathbf{K}$ is along $(\bar{1}10)$. φ describes a rotation around the (111) axis.

The dots in Fig. 2(c) show the predicted $E_1 - E_3$ doublet with a splitting of 4.0 μeV. Both lines are extremely narrow with a width $\lesssim 1$ μeV.

Having demonstrated qualitative agreement between theory and experiment, we proceed with the quantitative analysis of Δ_Q, Δ_3, and Δ_5. For $\mathbf{K} = (001)$, J_{ex}^Q and J_5 vanish and the fine structure is determined only by J_3. It should give rise to two lines, as E_1 and E_2 remain degenerate [Fig. 1(b)], where $E_{1,2}$ and E_3 are split by $3\Delta_3$. Indeed, the expected fine structure is observed in the experiment [Fig. 3(a)]. The levels $E_{1,2}$ and E_3 are distinguished by analyzing $|QA_{1,2}|^2$ and $|QA_3|^2$ as a function of $\mathbf{e}(\psi)$, which allows one to determine the sign of $\Delta_3 = -1.3$ μeV. In the angular range investigated no significant line shifts are expected and the degeneracy of E_1 and E_2 is only slightly lifted, which is masked by their spectral width. For the sample orientation of Fig. 2 E_1, E_2, and E_3 are shown as a function of φ in Fig. 3(b). $E_2 - E_1$ gives directly $\Delta_5 = 2$ μeV. Finally, $\Delta_Q = 5$ μeV is determined from E_3. These parameters also give the correct relative line positions, when comparing the absolute energies obtained for $\mathbf{K} = (001)$ to those for $\mathbf{K} = (\bar{1}10)$ [15].

As a test of consistency, we present data for $\mathbf{K} = (111)$ [Figs. 4(a)–4(d)]. According to Fig. 1(c) we expect for $\varphi \to 0$ a degenerate level $E_{1,2}$ plus a high energy state E_3. This is confirmed in Fig. 4(b). In agreement with theory $E_{1,2}$ splits into a doublet for $\varphi \neq 0$ [Figs. 4(a) and 4(c)]. As seen in Fig. 4(d) the $E_1 - E_2$ splitting increases with $|\varphi|$, while E_3 shows slight shifts. The fine structure is calculated (full lines) using the parameters obtained above. Obviously, the parameters allow a consistent description for these $\mathbf{K}$ directions. To overcome the line broadening found for lines with large $|QA|$ in Fig. 2(c) a thin sample had to be employed, which permits resolving the $E_1 - E_2$ splitting [Figs. 4(a) and 4(c)].

The degeneracy of the orthoexciton could also be lifted by strain. However, several arguments rule out an interpretation of the observed fine structure as strain-induced: (i) Strain is expected to be inhomogeneous across the sample. In our experiments, however, the spectrum is unaltered when probing various sections of the crystals. In 4 mm thick samples a macroscopic volume of the specimen is probed and strain would give rise to an inhomogeneous broadening. However the lines remain extremely narrow and Lorentzian in shape. (ii) The impact of residual strain can be approached by symmetry considerations: The strain tensor has the same symmetry as the SR exchange. Therefore the effect of strain on the Γ_5^+ states can be described by the three matrices ϵ_1, ϵ_3, ϵ_5, where each k_m in J_1, J_3, J_5 is replaced by a constant strain matrix element ε_m. Strain-induced shifts can be discriminated from exchange as they depend only on the orientation of the crystalline axes, but not on $\mathbf{K}$. Therefore, when turning the crystal one would not expect any dependence of the energy levels on φ for stain induced effects, contrary to the experimental results [Fig. 4(d)].

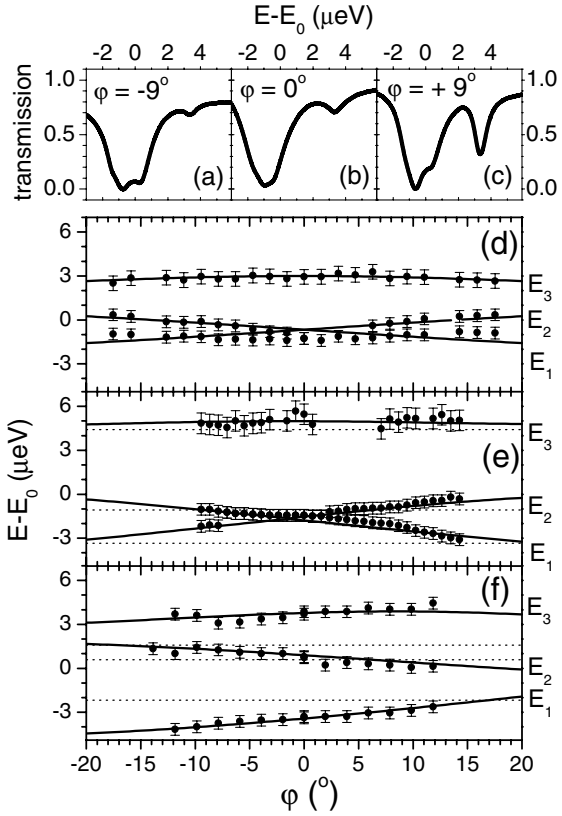

FIG. 4. Transmission spectra for $\varphi = -9°$ (a), 0 (b), and $+9°$ (c), where the sample (thickness 85 μm) was rotated around the $(11\bar{2})$ axis and **K** is along (111) at $\varphi = 0$. (d) E_1, E_2, and E_3 versus φ. (e) E_1, E_2, E_3 as a function of φ for a slightly strained sample [thickness 30 μm, $\mathbf{K} = (111)$ at $\varphi = 0$, axis of rotation $(11\bar{2})$]. (f) E_1, E_2, E_3 as a function of φ for a slightly strained sample [thickness 95 μm, $\mathbf{K} = (11\bar{2})$ at $\varphi = 0$, axis of rotation $(\bar{1}10)$]. In each case, full dots give the data, while full lines mark the theory. In (e) and (f) theory includes strain induced effects and the calculated strain offsets are given by the dotted lines.

This can be demonstrated by repeating the experiment of Figs. 4(a)–4(d) on a slightly strained sample [Fig. 4(e)]. The data show a significantly larger $E_{1,2} - E_3 \approx 7$ μeV ($\varphi = 0$) as compared to the unstrained sample. However, the same characteristic **K** dependence is found. Calculations including exchange and strain give a very good description of the data. For the exchange contribution the parameters derived above have been used. Obviously, the **K** dependence solely arises from exchange, while the increased splittings have to be attributed to stress induced offsets (dotted lines). As a crucial test of our analysis we have chosen a low symmetry K direction $(11\bar{2})$. As expected, we find three distinct lines with a pronounced φ dependence. Again slight strain-induced offsets are found (dotted lines), while the **K** dependencies of the orthoexciton energies are well described by our set of parameters.

In conclusion, we have derived and demonstrated K^2-dependent exchange interaction of excitons. For the yellow $1S$ orthoexcitons in Cu_2O the exchange parameters $\Delta_Q = 5 \pm 1.5$ μeV, $\Delta_3 = -1.3 \pm 0.2$ μeV, and $\Delta_5 = 2 \pm 0.3$ μeV are obtained, where the errors are estimated by evaluating several experiments performed on crystals of various thicknesses and orientations. The extremely sharp absorption resonances indicate long dephasing times (> 1.5 ns). Thus resonant single mode excitation might provide an efficient way to create a dense coherent population of dipole forbidden excitons.

The work was supported by the Deutsche Forschungsgemeinschaft and the QuIST program of DARPA.

[1] K. Cho, Phys. Rev. B **14**, 4463 (1976).
[2] G. L. Bir and G. E. Pikus, *Symmetry and Strain-Induced Effects in Semiconductors* (John Wiley and Sons, New York, 1974).
[3] E. L. Ivchenko and G. E. Pikus, *Superlattices and Other Heterostructures* (Springer-Verlag, Berlin, 1995).
[4] For an overview see M. Bayer *et al.*, Phys. Rev. B **65**, 195315 (2002), and references therein.
[5] See, e.g., U. Rössler and H. R. Trebin, Phys. Rev. B **23**, 1961 (1981); H. Fu, L.-W. Wang, and A. Zunger, Phys. Rev. B **59**, 5568 (1999).
[6] V. T. Agekyan, Phys. Status Solidi (a) **43**, 11 (1977).
[7] G. F. Koster *et al.*, *Properties of the Thirty-Two Point Groups* (MIT Press, Cambridge, MA, 1963).
[8] R. J. Elliott, Phys. Rev. **124**, 340 (1961).
[9] D. Fröhlich *et al.*, Phys. Rev. Lett. **67**, 2343 (1991).
[10] J. S. Schwinger *et al.*, *Classical Electrodynamics* (Perseus Books, Reading, MA, 1998).
[11] The LR exchange interaction was also recently analyzed by Moskalenko *et al.* [Phys. Status Solidi (b) **213**, 377 (1999)], who, however, treated it as an effective dipole-dipole interaction and did not take the off-diagonal matrix elements into account. As these are of the same magnitude as the diagonal terms, they should not be neglected.
[12] J. M. Luttinger, Phys. Rev. **102**, 1030 (1956).
[13] G. Kuwabara, M. Tanaka, and H. Fukutani, Solid State Commun. **21**, 599 (1977).
[14] Because of the thickness of the crystal the light is fully absorbed within a comparably broad spectral range.
[15] The use of a much larger set of data than shown here explains the small systematic discrepancies between experiment and theory in Fig. 3(b).